ACS APPLIED MATERIALS & INTERFACES

Research Article

www.acsami.org

Comparison of Nanocarbon–Silicon Solar Cells with Nanotube–Si or Graphene–Si Contact

Wenjing Xu,[†] Bing Deng,[‡] Enzheng Shi,[†] Shiting Wu,[†] Mingchu Zou,[†] Liusi Yang,[†] Jinquan Wei,[§] Hailin Peng,[‡] and Anyuan Cao*[,†]

[†]Department of Materials Science and Engineering, College of Engineering, and [‡]Center for Nanochemistry, Beijing Science and Engineering Center for Nanocarbons, Beijing National Laboratory for Molecular Sciences (BNLMS), College of Chemistry and Molecular Engineering, Peking University, Beijing 100871, People's Republic of China

[§]School of Materials Science and Engineering, State Key Laboratory of New Ceramics and Fine Processing, Key Laboratory of Materials Processing Technology of MOE, Tsinghua University, Beijing 100084, People's Republic of China

S *Supporting Information*

ABSTRACT: Nanocarbon structures such as carbon nanotubes (CNTs) and graphene (G) have been combined with crystalline silicon wafers to fabricate nanocarbon–Si solar cells. Here, we show that the contact between the nanocarbon and Si plays an important role in the solar cell performance. An asymmetrically configured CNT–G composite film was used to create either CNT–Si dominating or G–Si dominating junctions, resulting in obviously different solar cell behavior in pristine state. Typically, solar cells with direct G–Si contacts (versus CNT–Si) exhibit better characteristics due to improved junction quality and larger contact area. On the basis of the composite film, the obtained CNT–G–Si solar cells reach power conversion efficiencies of 14.88% under air mass 1.5, 88 mW/cm^2 illumination through established techniques such as acid doping and colloidal antireflection. Engineering the nanocarbon–Si contact is therefore a possible route for further improving the performance of this type of solar cells.

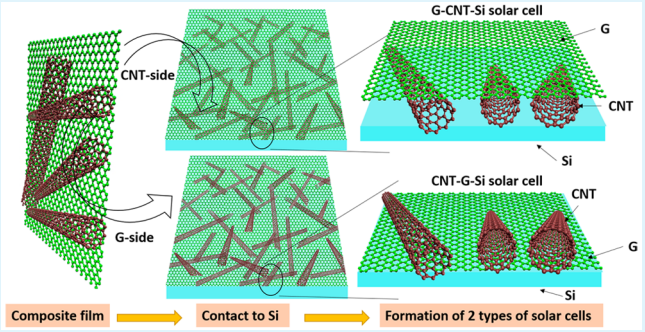

KEYWORDS: *nanocarbon–Si solar cell, carbon nanotube, graphene, contact, junction*

INTRODUCTION

Silicon solar cells possess high efficiency and stability, dominating the current photovoltaics market. Recently, nanocarbon materials such as carbon nanotubes (CNTs) and graphene (G) have been combined with crystalline Si to make nanocarbon–Si solar cells utilizing the excellent optoelectronic properties of both materials.[1−11] As compared to traditional Si cells based on a carefully engineered p–n junction, the nanocarbon–Si heterojuntion, obtained by directly depositing nanocarbon thin films onto the Si surface, becomes the key component of the nanocarbon–Si cells. Separate CNT and graphene films have been applied to Si to fabricate solar cells with power conversion efficiencies up to 14%–15%, as reported recently,[5,10] suggesting that both CNT–Si and G–Si contacts could work as charge separation junctions and lead to decent performance.

Despite that, the reported CNT and graphene films possess different microstructures. The former consists of an entanglement of individual CNTs (and bundles), while the latter, in ideal case, is a seamless two-dimensional plane. It is better to use "spider-web" or "network" to describe a CNT film given its porous network structure. Such a structural difference (together with related mechanical and electrical properties) results in distinct junction configurations, for example, linear contacts with partial surface coverage in CNT–Si cells versus planar G–Si contacts with full coverage. Now the question arises as to which type of contact is more favorable for achieving high efficiency devices? A direct comparison is yet available so far.

Here, we show that different nanocarbon–Si contacts indeed have certain influence on the solar cell characteristics. To clearly demonstrate this, an asymmetric composite film was constructed by placing a CNT network on one side of a graphene film, which was then made contact to Si at the CNT side or graphene side. Experimental tests reveal a better performance of the G–Si contact (versus CNT–Si) in the composite film–Si solar cells, which is analyzed on the basis of several key parameters related to junction quality. On the basis of the composite film, a CNT–G–Si solar cell was constructed, which could reach efficiencies up to 14.88% with the assistance of acid doping and colloidal antireflection.

Received: April 28, 2015
Accepted: July 27, 2015
Published: July 27, 2015

DOI: 10.1021/acsami.5b03699
ACS Appl. Mater. Interfaces 2015, 7, 17088–17094

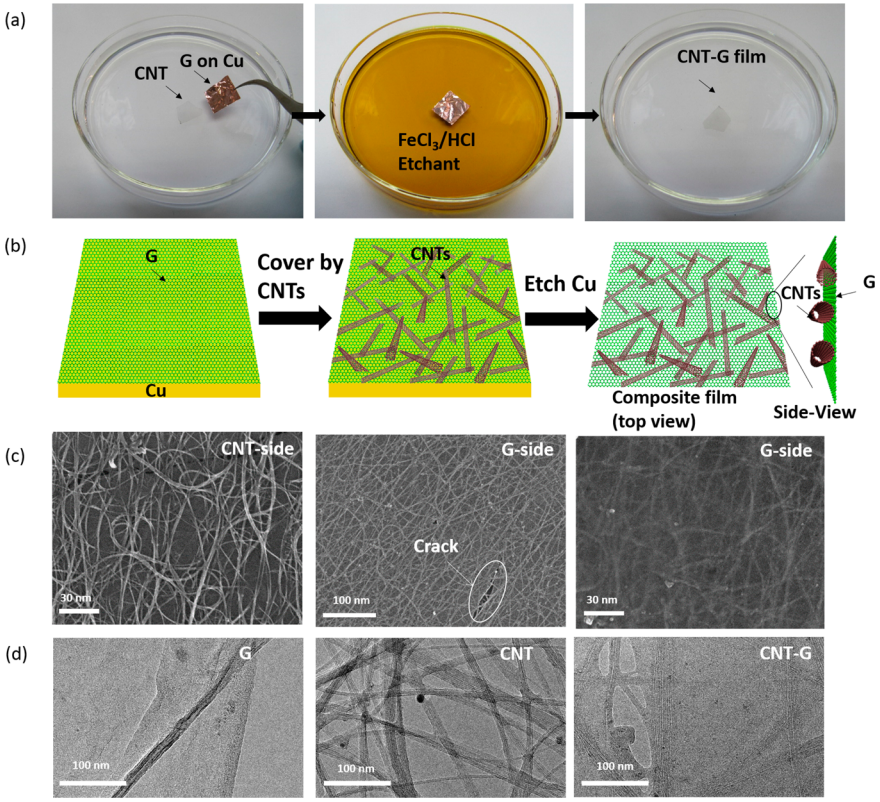

Figure 1. Fabrication and characterization of asymmetric CNT−G composite films. (a) Photos showing the process including (left) transferring a CNT film onto a Cu foil (with graphene on surface), (middle) etching the Cu foil, and (right) obtaining a freestanding CNT−G film on water. (b) Illustration of the fabrication process and the asymmetric structure of the composite film. (c) SEM images of the composite film from (left) the CNT side or (middle and right) the graphene side at different magnifications. (d) TEM images of (left) the graphene film, (middle) CNT network, and (right) composite film, respectively.

EXPERIMENTAL SECTION

Synthesis of CNTs and Graphene. First, we prepared large-area single-walled CNT films by a floating catalyst CVD method at 1160 °C. The precursor solution contained ferrocene and sulfur dissolved in xylene, with concentrations of 0.045 and 0.001 g/mL, respectively. The solution was injected into the upstream through a syringe pump at a rate of about 10 μL/min, and was carried by the flow of a mixture of hydrogen and argon (with volume fraction of H_2 15%) to the reaction zone. A typical reaction time was 30 min. By controlling the growing condition, we obtained very thin and highly transparent spiderweb-like CNT films, which are suspended at the downstream end of the CVD system. After the purification process with H_2O_2 (30 wt %) and HNO_3 (65 wt %) solution, we removed amorphous carbon and washed away the residue catalysts.

Graphene films were grown inside a 12-in. diameter horizontal tube furnace (Lindberg/Blue M) equipped with a 1-in. diameter quartz tube. Copper foil (Alfa Aesar, 99.8% purity, 25 μm thick) was placed on the quartz and loaded in the hot center of the furnace. The furnace was heated up to 1000 °C with the gas flow of H_2 50 sccm. After reaching 1000 °C, the copper was annealed for 30 min. The rate of H_2 and CH_4 was changed to 10 and 1 sccm, separately. The reaction was maintained 30 min for graphene growth. Finally, the copper was rapidly cooled at the speed of around 400 °C/min.

Fabrication of CNT−G Composite Films. The as-prepared CNT films were floated on the surface of deionized water and transferred onto Cu foils with as-grown graphene on both sides. After that, the Cu foils were dried on a thermal platform at 70 °C to ensure good adhesion and enhance interaction force between CNT and graphene. After the Cu foils were dried, $FeCl_3$/HCl solution (1 M/1 M in water) was used to remove the bottom graphene and etch the Cu foil. We then obtained large-area freestanding CNT−G composite thin films, floating on water surface.

Fabrication of CNT−G−Si Solar Cells and G−CNT−Si Solar Cells. We used n-type, 4-in. diameter, 400 μm-thick single-crystalline silicon wafers with 300 nm-thick oxide, and the bulk resistivity is 0.05−0.2 Ω cm. Windows with size of 3.3 mm (~0.11 cm^2 in area) were patterned through the photolithography technology. We then used the patterned Si wafer to pick up the asymmetrical composite film, with CNT or G in contact with Si, to form CNT−Si junctions in G−CNT−Si cells and G−Si junctions in CNT−G−Si cells, respectively. Micrometer-thick silver paste was used around the windows at the front; in contrast, we used liquid-state gallium−indium eutectic to form ohmic contact at the back. The electrodes were extracted by Ag wires.

Characterization. The structure and morphology of CNTs, G, and CNT−G composite films were characterized by SEM (Hitachi S4800), TEM (FEI Tecnai G2 T20), and Raman spectrometry (Renishaw inVia plus). A RTS-4 four-probe meter was used to measure the sheet resistance of CNTs, G, and the composite films. The transmittance was measured by a UV−vis−NIR spectrophoeometer (Agilent Cary 5000). Solar cell characteristics were tested by a solar simulator (New Thermo Oriel 91195A-1000) under 0.88 sun (AM 1.5) and a source meter (Keithley 2635A).

RESULTS AND DISCUSSION

Figure 1 illustrates the fabrication process of CNT−graphene composite films with asymmetric structure, that is, all CNTs on one side and graphene on the other side. Large-area single-walled nanotube spider-webs in freestanding form, and single- to few-layer graphene grown on Cu substrate, were synthesized by chemical vapor deposition (CVD), respectively.[11−15] The composite film was made by transferring a CNT spider-web to the graphene surface and then etching away the Cu foil (see

DOI: 10.1021/acsami.5b03699
ACS Appl. Mater. Interfaces 2015, 7, 17088−17094

Experimental Section for details). To ensure good adhesion between CNTs and graphene, the spider-web was collapsed onto the Cu foil by aqueous transfer and mild annealing, forming intimate contact with graphene. The resulting CNT−G composite films can float on the water surface and be picked up by particular substrates such as silicon wafers (Figure 1a). The composite film has excellent flexibility and can be twisted into straight yarns and entangled structures upon overtwisting (Figure S1). From a structural point of view, all CNTs are located on one side (the top surface of graphene during CVD growth on Cu foil), which is considered as an "asymmetric" composite film (Figure 1b). This structure is different from previously reported hybrid films in which dispersed CNTs are embedded within graphene,[16−18] or graphene layer supported by a multiwalled nanotube sheet (spun from a superaligned forest) resembling insect wings.[19,20]

We have examined the CNT−G composite film by scanning electron microscopy (SEM) and transmission electron microscopy (TEM) characterization. To do this, a composite film was suspended on an Al mesh (with 3 × 2 mm^2 holes) so that both sides of the sample could be viewed. From the CNT side, the interconnected CNT bundles like a spider-web are clearly seen, forming a porous network (Figure 1c), while from the other side, a large graphene layer is present on top of the CNT network, making the underlying CNTs less clear. Sometimes there are several CNTs exposed from small cracks in the graphene plane. A close view reveals that most of the graphene area is seamless, which prevents penetration by CNTs; this is an important feature that ensures no CNTs can make direct contact to Si from the graphene side. Three samples were prepared for TEM characterization, including a graphene sample removed from Cu, an as-grown CNT spider-web consisting of single-walled nanotube bundles with diameters of several to tens of nanometers, and a composite film (Figure 1d). In the composite film, porous areas among the CNT network have been covered by a graphene layer. It seems that our solution transfer method results in good integration of the CNT bundles and graphene, without cracks or gaps at their interface. This brings desired mechanical and electrical properties to the composite film (as discussed later) for photovoltaic applications.

The composite structure was also characterized by Raman spectroscopy. Original CNT spider-webs show typical radial breathing mode (RBM) peaks in the range of 100−300 cm^{-1}, while the CVD-grown graphene exhibits a strong 2D band with the intensity ratio to the G band (I_{2D}/I_G) of ∼1.77, indicating that this sample consists of primarily mono- to few-layer domains, consistent with the TEM images. The Raman spectrum of the composite film possesses a combination of features from CNTs and graphene (Figure 2a). The D band remains low, indicating that the composite fabrication process has not induced more defects.

We have further performed electrical and optical measurements on the composite films. Attaching a CNT spider-web onto graphene improves its electrical conductivity substantially. Our graphene sample has a four-probe sheet resistance of about 1500 Ω/□, whereas that of CNTs is in the range of 66.95−325 Ω/□ (depending on the spider-web thickness). As a result, the corresponding CNT-G films have sheet resistances of 52.63−240 Ω/□, much lower than separate CNT or graphene samples (Figure 2b, Table S1). This is because the parallel configuration of CNT−G composite provides additional carrier

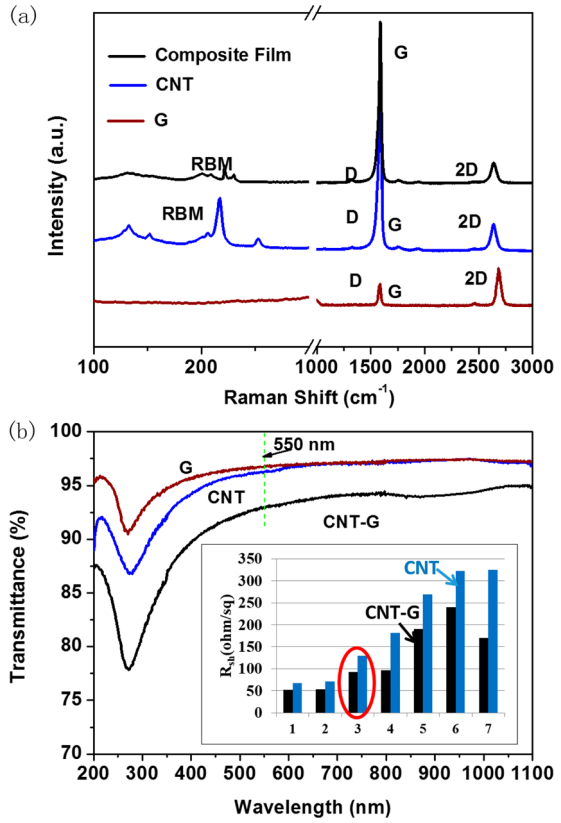

Figure 2. Spectroscopy characterization of CNT−G composite films. (a) Raman spectra of a graphene film, a CNT network, and a CNT−G composite film. (b) Optical transmittance of the graphene, CNT, and composite films. Inset is a list of sheet resistances of several CNT films (blue columns) and CNT−G composite films (black columns) with different thicknesses measured from samples #1 to #7. The transmittance curves correspond to sample #3 (red circle).

transport paths due to the continuous graphene plane and CNT network, as well as their good contact interface.

At the same time, optical absorption was carried out on three selected samples, original graphene, CNT spider-web, and the composite film with sheet resistances of 1500, 129.2, and 93.05 Ω/□, respectively (Figure 2b). The transmittance of the composite film, due to simple overlapping of the two layers, decreases to 93.02% (at 550 nm) as compared to that of the graphene only (∼96.75%) and the CNT spider-web (96.27%). Thus, the combination of CNTs and graphene has improved the film conductivity but also leads to slight loss of transparency.

To compare the solar cell behavior, these nanocarbon films were transferred to n-type single-crystalline silicon wafers to make nanocarbon-Si cells, as described in our previous reports.[1,6] Here, because of the asymmetric structure of the composite film, two different sandwich-like structures (CNT−G−Si, G−CNT−Si) have been obtained, depending on which side was made into contact with Si (illustrated in Figure 3a, Figure S2). In the case of CNT−G−Si, the graphene side was coated on Si, which also prevented CNTs from contacting Si; therefore, the G−Si junction should dominate the cell behavior. The G−CNT−Si structure is relatively complex as both CNT−Si and G−Si junctions coexist in the cell. This is because the top graphene cover, which is a flexible sheet, may access the Si surface through the porous CNT network. However, it leads to incomplete contact between the suspended graphene layer and

DOI: 10.1021/acsami.5b03699
ACS Appl. Mater. Interfaces 2015, 7, 17088−17094

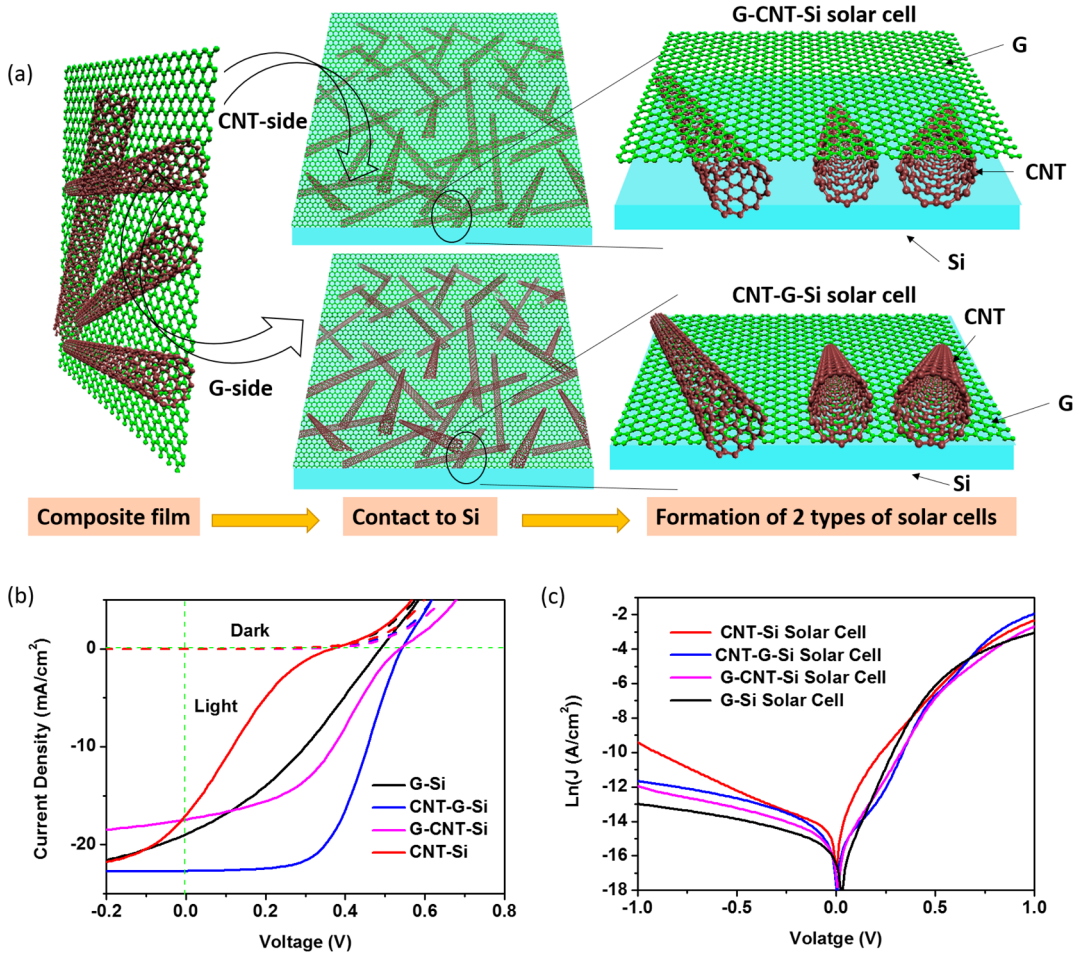

Figure 3. CNT−G composite film−Si solar cells. (a) Illustration of the fabrication process, in which either the CNT-side or graphene-side of the composite film was made into direct contact to Si, resulting in two types of solar cells (G−CNT−Si and CNT−G−Si). (b) Dark and light J−V characteristics of different solar cell structures including G−Si, CNT−Si, G−CNT−Si, and CNT−G−Si. (c) Semilog plots of J−V curves of the above four types of solar cells.

Si; therefore, we consider that the CNT−Si contact still dominates in such mixed junctions. No matter which side is placed on the top (or bottom), the electrical conductivity and optical transparency of the composite films would not change, allowing a comparative study on those two junctions.

Solar cell samples made from individual nanocarbon (CNT−Si, G−Si) or composite films with different contact sides (CNT−G−Si, G−CNT−Si) have been tested under the same conditions (air mass 1.5, 88 mW/cm^2, all cells have the same active area 3.3 × 3.3 mm^2). All devices are tested in pristine state, that is, without acid doping or adding antireflection layer. In general, solar cells incorporating composite films show more desired current density−voltage (J−V) characteristics than cells using single nanocarbon films (Figure 3b, Table S2). Specifically, the CNT−G−Si and G−CNT−Si cells have better fill factors (FF) and open-circuit voltages (V_{oc}). For example, a CNT−G−Si cell has a V_{oc} of 0.54 V, a short-circuit current density (J_{sc}) of 22.69 mA/cm^2, a FF of 57%, and a power conversion efficiency (η) of 7.97%, whereas a G−Si cell (without CNTs on the top) shows a V_{oc} of 0.49 V, a J_{sc} of 18.83 mA/cm^2, and a FF of 33%, resulting in a lower η of 3.47%. Higher FF values in the composite film−Si cells could be attributed to the improved electrical conductivity (thus, reduced series resistance) after combining CNTs and graphene. Furthermore, dark measurements provide more information on key parameters such as the saturation current density (J_s) and the diode ideality factor (n), based on the equation $J(T,V) = J_s(T)[\exp(qV/nk_BT) - 1]$, where $J(T,V)$ is the current density across the nanocarbon−Si interface at certain temperature (T) and voltage (V), q is the electronic charge, and k_B is the Boltzmann constant. A linear fitting of ln J versus V in the same regime (0.3−0.5 V) generates specific values of J_s and n of the above four cells, which follow that J_s(CNT−G−Si) < J_s(G−CNT−Si) < J_s(G−Si) < J_s(CNT−Si) as well as n(CNT−G−Si) < n(G−CNT−Si) < n(G−Si) < n(CNT−Si) (Figure 3c, Table S3). A consistent trend is found in the above four types of solar cells, in which the ideality factor of a diode should degrade (n increases correspondingly) as J_s increases. A larger J_s indicates more severe recombination in the junction and the bulk of solar cells. Typically, the G−Si contact makes a better diode than the CNT−Si structure, and the CNT−G−Si junction shows both the lowest J_s (36 nA/cm^2) and n (1.80), which also has the highest cell efficiency. In addition, the relationship of $V_{oc} = kT/q \cdot \ln(J_{sc}/J_s)$ dictates that V_{oc} would increase as J_s drops, which is consistent with our experimental measurements. The V_{oc} is 0.54, 0.53, 0.49, and 0.36 V for cells made from CNT−G, G−CNT, G, and CNT films, respectively (Figure 3a).

For solar cells made with composite films, their performances also depend on which side of the composite film is in direct contact to Si. When the graphene side contacts Si, the resulting

DOI: 10.1021/acsami.5b03699
ACS Appl. Mater. Interfaces 2015, 7, 17088−17094

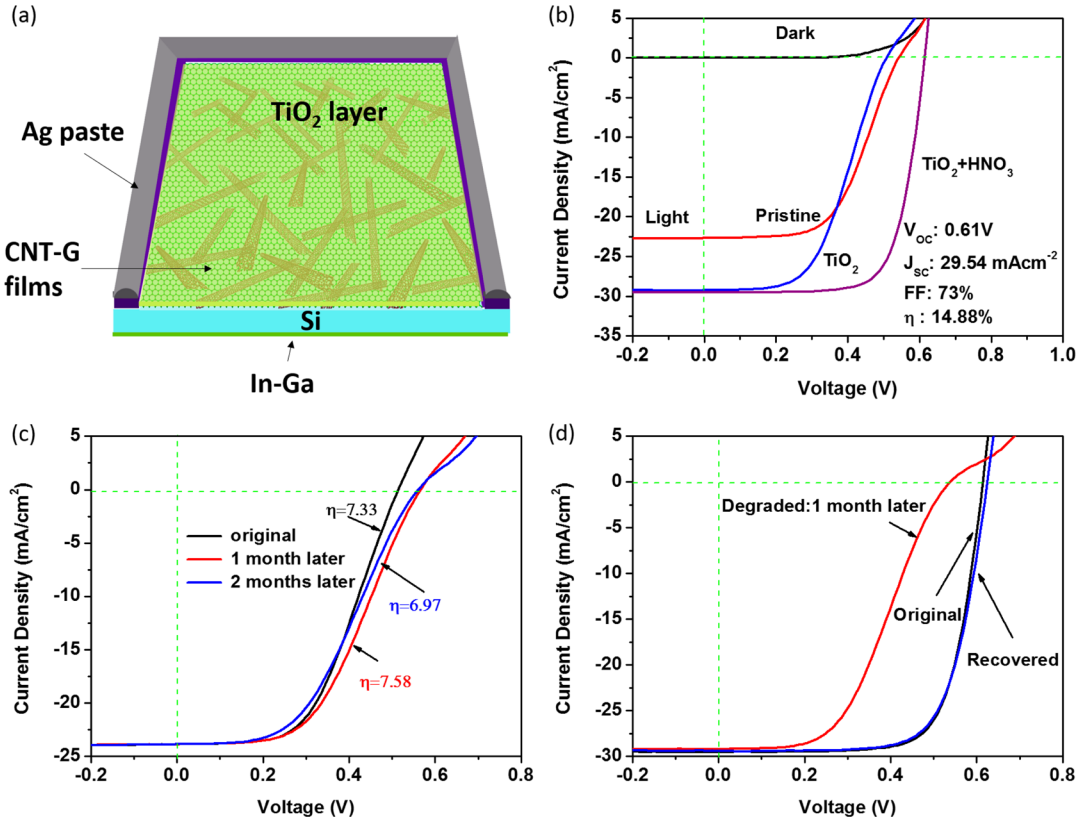

Figure 4. High-efficiency CNT−G−Si solar cells by optimization. (a) Illustration of an optimized solar cell consisting of an antireflection TiO_2 layer coated on the CNT−G film, enclosed by silver paste as top electrode and In−Ga as back electrode. (b) J−V curves of a CNT−G−Si cell in pristine state, after coating TiO_2, and after HNO_3 doping, respectively. (c) J−V curves of a pristine CNT−G−Si cell (without TiO_2 and HNO_3 doping) in original state and after 1 and 2 months storage, respectively. (d) J−V curves of an optimized CNT−G−Si cell (with TiO_2 and HNO_3 doping) in original state, after 1 month storage (showing degradation), and after recovery by HNO_3 doping again, respectively.

cells (CNT−G−Si) generally produce higher efficiencies (in the range of 7.2%−8.1%) than the G−CNT−Si cells (η < 6.0%) (Figure S3, Table S5). There are two structural factors that may explain this difference. First, the dominating junction is G−Si in CNT−G−Si cells, while in the latter the CNT−Si junction dominates, and the G−Si junction leads to better diode properties (lower J_s and n). Second, there is more effective junction area (with built-in electric field) in the CNT−G−Si cells, due to full surface coverage, than the G−CNT−Si cell containing an intermediate porous CNT network. As a result, the CNT−G−Si is a preferred structure for improving the diode quality and solar cell performance.

Optical and electrical properties of CNT films are highly dependent on the film thickness, which will determine the performance of CNT-incorporated solar cells, and an optimal film thickness for maximum cell efficiency might exist.[21] We have carried out further experiments on different film thicknesses. Solar cells with two relatively thick CNT films (with decreased optical transparencies of 84.8% and 74.7%, respectively) have been made and tested (Figure S4). The results indicate that the G−Si junction is better than the CNT−Si junction as a generalized conclusion, for CNT films with different thicknesses (or transmittances). Also, as the film thickness increases (transmittance decreases from >90% to 84.8% and 74.7%), the solar cell efficiency drops consistently. For thicker films, CNTs are overlapped into multilayers, but the film remains highly porous. This is not very effective in improving the CNT−Si junction area, and cannot compensate the loss of optical transparency. Therefore, a relatively thin CNT film (hence higher transparency) is more desired for making CNT (or G)−Si solar cells.

The performance of solar cells could be further improved by adding an antireflection layer and doping of nanocarbon films. Previously, we have used a TiO_2 colloidal layer and acid doping on CNT−Si or G−Si cells to improve their efficiencies up to about 15%.[5,10] Here, our composite film−Si cells are also amenable to those techniques and exhibit significant enhancement. A TiO_2 colloid solution was first spin-coated onto the CNT−G−Si cell to form a thin antireflection layer (~60 nm), and then the cell was placed downward on HNO_3 vapor for 15 s (as illustrated in Figure 4a). The J−V characteristics show an increase of J_{sc} (from 22.69 to 29.54 mA/cm^2) after the TiO_2 coating step, and simultaneous improvement of FF (from 57% to 73%) and V_{oc} (from 0.54 to 0.61 V) after HNO_3 doping (Figure 4b, Table S4). Finally, the CNT−G−Si cell achieved a power conversion efficiency of 14.88% (air mass 1.5, 88 mW/cm^2). Currently, the cell efficiency generated from our composite films does not surpass the highest records obtained from individual CNT or graphene films, but further progress might be possible by using high-quality single-layer graphene and optimizing the process for making composite films. We also tested the incident photon to current conversion efficiency (IPCE) of the CNT−G−Si solar cell in pristine state and TiO_2 colloidal layer (Figure S5).

At last, we investigated the stability of the composite film−Si solar cells stored in ambient conditions over a long time. In the pristine state (without antireflection or doping), the CNT−G−Si cell has a relatively low efficiency but excellent stability. As

DOI: 10.1021/acsami.5b03699
ACS Appl. Mater. Interfaces 2015, 7, 17088−17094

shown in the $J-V$ characteristics, a fresh cell showed an original efficiency of 7.33%, which increased to 7.58% after 1-month storage and then decreased to 6.96% after 2 months (Figure 4c). Interaction with air (oxygen) is the underlying mechanism, in which oxygen doping of CNTs and G could improve cell efficiency, whereas the growth of oxides at the Si surface may cause degradation.[22−24] In contrast, for the CNT−G−Si cell with TiO_2 coating and subjected to HNO_3 doping (tested in Figure 4b), its efficiency dropped from 14.88% to 8.44% after 1-month storage (Figure 4d). The decreasing FF and V_{oc} (due to HNO_3 vaporization and loss of doping effects) are the main reasons causing the degradation, whereas the current density remains stable. The cell efficiency can be recovered to the original value by HNO_3 treatment again, indicating that this type of acid doping is not stable but rather a reversible process.

CONCLUSION

We have studied nanocarbon composite film−Si solar cells with different configurations, in which either a porous CNT network or a planar graphene sheet was made into contact with Si. The results show that the graphene−Si contact results in better junction characteristics and enhanced cell efficiency as compared to the CNT−Si contact. A CNT−G−Si cell with optimized structure reaches an efficiency of 14.88%, and there remains much room for further improvement. Engineering nanocarbon composite films with appropriate contact to Si, by considering the structural difference between CNTs and graphene, is a potential way to design and fabricate high performance nanocarbon−Si solar cells.

ASSOCIATED CONTENT

Supporting Information

The Supporting Information is available free of charge on the ACS Publications website at DOI: 10.1021/acsami.5b03699.

Sheet resistances of CNT and composite films; specific parameters and efficiencies of different types of solar cells; linear fitting of dark characteristics; SEM characterization of the solar cell morphology; $J-V$ characteristics of more composite film−Si solar cells; measurements on composite film−Si solar cells made with different CNT film thicknesses; IPCE tests (PDF)

AUTHOR INFORMATION

Corresponding Author

*E-mail: anyuan@pku.edu.cn.

Notes

The authors declare no competing financial interest.

ACKNOWLEDGMENTS

This work was financially supported by the National Nature Science Foundation of China (NSFC 51325202).

REFERENCES

(1) Wei, J. Q.; Jia, Y.; Shu, Q. K.; Gu, Z. Y.; Wang, K. L.; Zhuang, D. M.; Zhang, G.; Wang, Z. C.; Luo, J. B.; Cao, A. Y.; Wu, D. H. Double-Walled Carbon Nanotube Solar Cells. *Nano Lett.* **2007**, *7*, 2317−2321.

(2) Jia, Y.; Wei, J. Q.; Wang, K. L.; Cao, A. Y.; Shu, Q. K.; Gui, X. C.; Zhu, Y. Q.; Zhuang, D. M.; Zhang, G. B. B.; Ma, L. D.; Wang, W. J.; Liu, Z. C.; Wang, J. B.; Luo; Wu, D. Nanotube-Silicon Heterojunction Solar Cells. *Adv. Mater.* **2008**, *20*, 4594−4598.

(3) Li, X. K.; Gittleson, F.; Carmo, M.; Sekol, R. C.; Taylor, A. D. Scalable Fabrication of Multifunctional Freestanding Carbon Nanotube/Polymer Composite Thin Films for Energy Conversion. *ACS Nano* **2012**, *6*, 1347−1356.

(4) Jung, Y.; Li, X. K.; Rajan, N. K.; Tayor, A. D.; Reed, M. A. Record High Efficiency Single-Walled Carbon Nanotube/Silicon p-n Junction Solar Cells. *Nano Lett.* **2013**, *13*, 95−99.

(5) Shi, E. Z.; Zhang, L. H.; Li, Z.; Li, P. X.; Shang, Y. Y.; Jia, Y.; Wei, J. Q.; Wang, K. L.; Zhu, H. W.; Wu, D. H.; Zhang, S.; Cao, A. Y. TiO_2-coated Carbon Nanotube-Silicon Solar Cells with Efficiency of 15%. *Sci. Rep.* **2012**, *2*, 884−888.

(6) Li, X. M.; Zhu, H. W.; Wang, K. L.; Cao, A. Y.; Wei, J. Q.; Li, C. Y.; Jia, Y.; Li, Z.; Li, X.; Wu, D. H. Graphene-on-Silicon Schottky Junction Solar Cells. *Adv. Mater.* **2010**, *22*, 2743−2748.

(7) Li, X.; Fan, L. L.; Li, Z.; Wang, K. L.; Zhong, M. L.; Wei, J. Q.; Wu, D. H.; Zhu, H. W. Boron Doping of Graphene for Graphene-Silicon p-n Junction Solar Cells. *Adv. Energy Mater.* **2012**, *2*, 425−429.

(8) Li, X. M.; Xie, D.; Park, H.; Zhu, M.; Zeng, T. H.; Wang, K. L.; Wei, J. Q.; Wu, D. H.; Kong, J.; Zhu, H. W. Ion Doping of Graphene for High-Efficiency Heterojunction Solar Cells. *Nanoscale* **2013**, *5*, 1945−1948.

(9) Miao, X. C.; Tongay, S.; Petterson, M. K.; Berke, K.; Rinzler, A. G.; Appleton, B. R.; Hebard, A. F. High Efficiency Graphene Solar Cells by Chemical Doping. *Nano Lett.* **2012**, *12*, 2745−2750.

(10) Shi, E. Z.; Li, H. B.; Yang, L.; Zhang, L. H.; Li, Z.; Li, P. X.; Shang, Y. Y.; Wu, S. T.; Li, X. M.; Wei, J. Q.; Wang, K. L.; Zhu, H. W.; Wu, D. H.; Fang, Y.; Cao, A. Y. Colloidal Antireflection Coating Improves Graphene-Silicon Solar Cells. *Nano Lett.* **2013**, *13*, 1776−1781.

(11) Song, L.; Ci, L.; Lv, L.; Zhou, Z. P.; Yan, X. Q.; Liu, D. F.; Yuan, H. J.; Gao, Y.; Wang, J. X.; Liu, L. F.; Zhao, X. W.; Zhang, Z. X.; Dou, X. Y.; Zhou, W. Y.; Wang, G.; Wang, C. Y.; Xie, S. S. Direct Synthesis of a Macroscale Single-Walled Carbon Nanotube Non-Woven Material. *Adv. Mater.* **2004**, *16*, 1529−1534.

(12) Wei, J. Q.; Zhu, H. W.; Li, Y. H.; Chen, B.; Jia, Y.; Wang, K. L.; Wang, Z. C.; Liu, W. J.; Luo, J. B.; Zheng, M. X.; Wu, D. H.; Zhu, Y. Q.; Wei, B. Q. Ultrathin Single-Layered Membranes from Double-Walled Carbon Nanotubes. *Adv. Mater.* **2006**, *18*, 1695−1700.

(13) Dan, B.; Irvin, G. C.; Pasquali, M. Continuous and Scalable Fabrication of Transparent Conducting Carbon Nanotube Films. *ACS Nano* **2009**, *3*, 835−843.

(14) Li, X. S.; Cai, W. W.; An, J. H.; Kim, S.; Nah, J.; Yang, D. X.; Piner, R.; Velamakanni, A.; Jung, I.; Tutuc, E.; Banerjee, S. K.; Colombo, L.; Ruoff, R. S. Large-Area Synthesis of High-Quality and Uniform Graphene Films on Copper Foils. *Science* **2009**, *324*, 1312−1314.

(15) Bae, S.; Kim, H.; Lee, Y.; Xu, X. F.; Park, J. S.; Zheng, Y.; Balakrishnan, J.; Lei, T.; Kim, H. R.; Song, Y. I.; Kim, Y. J.; Kim, K. S.; Ozyilmaz, B.; Ahn, J. H.; Hong, B. H.; Iijima, S. Roll-to-Roll Production of 30-in. Graphene Films for Transparent Electrodes. *Nat. Nanotechnol.* **2010**, *5*, 574−578.

(16) Yan, Z.; Peng, Z. W.; Casillas, G.; Lin, J.; Xiang, C. S.; Zhou, H. Q.; Yang, Y.; Ruan, G. D.; Raji, A. R. O.; Samuel, E. L.; Hauge, G. R. H.; Yacaman, M. J.; Tour, J. M. Rebar Graphene. *ACS Nano* **2014**, *8*, 5061−5068.

(17) Kim, S. H.; Song, W.; Jung, M. W.; Kang, M. A.; Kim, K.; Chang, S. J.; Lee, S. S.; Lim, J.; Hwang, J.; Myung, S.; An, K. S. Carbon Nanotube and Graphene Hybrid Thin Film for Transparent Electrodes and Field Effect Transistors. *Adv. Mater.* **2014**, *26*, 4247−4252.

(18) Nguyen, D. D.; Tiwari, R. N.; Matsuoka, Y.; Hashimoto, G.; Rokuta, E.; Chen, Y. Ze.; Chueh, Y. L.; Yoshimura, M. Low Vacuum Annealing of Cellulose Acetate on Nickel Towards Transparent Conductive CNT−Graphene Hybrid Films. *ACS Appl. Mater. Interfaces* **2014**, *6*, 9071−9077.

(19) Lin, X. Y.; Liu, P.; Wei, Y.; Li, Q. Q.; Wang, J. P.; Wu, Y.; Feng, C.; Zhang, L. N.; Fan, S. S.; Jiang, K. L. Development of an Ultra-Thin Film Comprised of a Graphene Membrane and Carbon Nanotube Vein Support. *Nat. Commun.* **2013**, *4*, 2920−2924.

(20) Kholmanov, I. N.; Magnuson, C. W.; Piner, R.; Kim, J.-Y.; Aliev, A. E.; Tan, C.; Kim, T. Y.; Zakhidov, A. A.; Sberveglieri, G.;

DOI: 10.1021/acsami.5b03699
ACS Appl. Mater. Interfaces 2015, 7, 17088−17094

Baughman, R. H.; Ruoff, R. S. Optical, Electrical and Eledtromechanical Properties of Hybrid Graphene/Carbon Nanotube Films. *Adv. Mater.* **2015**, *27*, 3053−3059.
(21) Li, X.; Jung, Y.; Sakimoto, K.; Goh, T. − H.; Reed, M. A.; Taylor, A. D. Improved Efficiency of Smooth and Aligned Single Walled Carbon Nanotube/Silicon Hybrid Solar Cells. *Energy Environ. Sci.* **2013**, *6*, 879−887.
(22) Li, X.; Huang, J. S.; Nejati, S.; McMillon, L.; Huang, S.; Osuji, C. O.; Hazari, N.; Taylor, A. D. Role of HF in Oxygen Removal from Carbon Nanotubes: Implications for High Performance Carbon Electronics. *Nano Lett.* **2014**, *14*, 6179−6184.
(23) Jia, Y.; Cao, A. Y.; Kang, F. Y.; Li, P. X.; Gui, X. C.; Zhang, L. H.; Shi, E. Z.; Wei, J. Q.; Wang, K. L.; Zhu, H. W.; Wu, D. H. Strong and Reversible Modulation of Carbon Nanotube-Silicon Heterojunction Solar Cells by an Interfacial Oxide Layer. *Phys. Chem. Chem. Phys.* **2012**, *14*, 8391−8396.
(24) Song, Y.; Li, X. M.; Mackin, C.; Zhang, X.; Fang, W. J.; Palacios, T.; Zhu, H. W.; Kong, J. Role of Interfacial Oxide in High-Efficiency Graphene−Silicon Schottky Barrier Solar Cells. *Nano Lett.* **2015**, *15*, 2104−2110.

DOI: 10.1021/acsami.5b03699
ACS Appl. Mater. Interfaces 2015, 7, 17088−17094